IOP Publishing Journal of Physics B: Atomic, Molecular and Optical Physics

J. Phys. B: At. Mol. Opt. Phys. **45** (2012) 165503 (15pp) doi:10.1088/0953-4075/45/16/165503

Stability of linear and nonlinear lambda and tripod systems in the presence of amplitude damping

Viktoras Pyragas[1,2] **and Gediminas Juzeliūnas**[1]

[1] Institute of Theoretical Physics and Astronomy of Vilnius University, A Gostauto 12, LT-01108 Vilnius, Lithuania

[2] Semiconductor Physics Institute of Center for Physical Sciences and Technology, A Gostauto 11, LT-01108 Vilnius, Lithuania

E-mail: viktpy@pfi.lt and gediminas.juzeliunas@tfai.vu.lt

Received 22 February 2012, in final form 25 June 2012
Published 25 July 2012
Online at stacks.iop.org/JPhysB/45/165503

Abstract

We present the stability analysis of the dark states in the adiabatic passage for the linear and nonlinear lambda and tripod systems in the presence of amplitude damping (losses). We perform an analytic evaluation of the real parts of eigenvalues of the corresponding Jacobians, the non-zero eigenvalues of which are found from the quadratic characteristic equations, as well as by the corresponding numerical simulations. For nonlinear systems, we evaluate the Jacobians at the dark states. Similar to the linear systems, here we also find the non-zero eigenvalues from the characteristic quadratic equations. We reveal a common property of all the considered systems showing that the evolution of the real parts of eigenvalues can be split into three stages. In each of them, the evolution of the stimulated Raman adiabatic passage is characterized by different effective dimension. This results in a possible adiabatic reduction of one or two degrees of freedom.

1. Introduction

Over the last couple of decades, there has been a continuing interest in the stimulated Raman adiabatic passage (STIRAP) [1–5]. The simplest situation is the adiabatic passage in a linear lambda system [6–12] containing a single dark (uncoupled) state which is immune to the atom–light coupling. If the atomic initial and final states are the ground states representing the dark states of the system, the atom can be transferred between these two states by slowly changing the relative intensity of the laser pulses. When the adiabatic passage is slow enough, the excited state is only slightly populated and thus the losses are minimum. The analysis has been extended for the STIRAP process in the tripod system characterized by two dark states [13–15]. This enables us to create a quantum superposition of metastable states out of a single initial state in a robust and coherent way [16, 17]. The schemes involving more atomic and molecular levels were also proposed for the creation of a superposition of states [18] as well as for the experimental control of excitation flow [19]. Recently, the treatment was further extended to the nonlinear lambda [20–31] and tripod [32] schemes.

Usually, the STIRAP is based on the adiabatic approximation. However, one has to distinguish between the adiabatic approximation and the adiabatic reduction of dynamic systems. In quantum mechanics, a closed quantum system is said to undergo adiabatic dynamics if its Hilbert space can be decomposed into decoupled Schrödinger eigenspaces with distinct, time-continuous and non-crossing instantaneous eigenvalues of Hamiltonian. On the other hand, an open quantum system is said to undergo adiabatic dynamics if its Hilbert–Schmidt space can be decomposed into decoupled Lindblad–Jordan eigenspaces with distinct, time-continuous and non-crossing instantaneous eigenvalues of the Lindblad superoperator [33]. The system is called adiabatically approximated if the error term in the Schrödinger equation (for closed systems) or in the master equation (for open systems) is much less than the diagonalyzed part; i.e. one may neglect the non-diagonal terms in order to obtain an adiabatically approximated version of the system. Note that in the presence of fast-driven oscillations, some additional

conditions (in addition to the slowness of the evolution of the Hamiltonian) have to be imposed [34].

Another procedure is the adiabatic elimination of decaying degrees of freedom. It is related to the dynamic systems in which some degrees of freedom may decay. In accordance with this definition, these degrees of freedom may be adiabatically eliminated by solving the corresponding algebraic equations; the rhs of decaying equations is set to be equal to zero. Consequently, one obtains the dependencies of decaying variables on the remaining ones. If there are several decaying variables, one may eliminate them one by one, starting from the fastest variable and finishing with the slowest one. Such a procedure can be found e.g. in the book by Haken [35].

The aim of this work is to perform a stability analysis of the dark states in the adiabatic passage for the linear and nonlinear lambda and tripod systems. The analysis sets limits to the adiabatic reduction of the systems. Moreover, we have revealed that in all the considered systems, the stability properties of the dark states are similar, namely there are three time intervals with a different number of the negative real parts of the Jacobians. This suggests that the corresponding linear and nonlinear systems have equal possibilities of adiabatic reduction. Although the linear lambda [1–12] and tripod systems [13–17, 36] have been substantially studied in the literature, here we apply our treatment also to these linear setups in order to facilitate the subsequent analysis of the nonlinear systems.

The nonlinear lambda system can be realized in the Bose–Einstein condensates (BEC) via photoassociation (PA) from a dissociated (quasicontinuum) atomic state to the ground molecular state in the presence of the intermediate molecular state [20, 21]. The aim of the quantum control is to transfer the whole population from the dissociated atomic to the ground molecular state. One thus creates ultracold molecules by associating cold atoms [29, 37]. In this case, the dark state is a generalization of that for the linear systems. In the linear case, the dark state is defined as a superposition of the initial and target ground atomic states which corresponds to the zero eigenergy of the system Hamiltonian. The same dark state may also be defined as a steady-state solution of the Schrödinger equation. If we consider the nonlinear system, we can again define the dark state as a steady state [29] of the equations of motion following from the Heisenberg equation. In the nonlinear systems, the behaviour of the dark state reproduces that in the linear systems although the superposition is missing now. We thus obtain the nonlinear version of STIRAP: the entire population is distributed among the steady-state probability amplitudes of the initial atomic and the target molecular state. At the beginning the whole population is atomic, whereas at the end it is in the ground molecular state.

Different from the traditional STIRAP in an atomic lambda system, the atom–molecule STIRAP contains nonlinearities originating from the conversion process of atoms to molecules, as well as from the interparticle interactions described by the nonlinear mean-field contributions. The existence of such nonlinearities makes it difficult to analyse the adiabaticity of the atom–molecule conversion systems due to the absence of the superposition principle. In the STIRAP, the linear instability could make the quantum evolution deviate from the dark state rapidly even in the adiabatic limit [22]. Therefore, it is important to avoid such an instability for the efficiency of the STIRAP.

The nonlinear tripod system can be realized in the PA with two target states involved. Specifically, one may consider the atom–molecule transition in ultracold quantum gases via PA. It was first considered in [32] where the second-order dynamic system was derived that parametrizes the solution evolving on the dark-state manifold. However, the stability of the solution moving along the manifold was not considered. Therefore, we shall check the stability of this solution, i.e. see whether the nearby solutions are attracted back to this manifold.

The adiabatic theory for nonlinear quantum systems was first discussed by Liu *et al* [38] who obtained the adiabatic conditions and adiabatic invariants by representing the nonlinear Heisenberg equation in terms of an effective classical Hamiltonian. Pu *et al* [23] and Ling *et al* [24] extended such an adiabatic theory to the atom–dimer conversion system by linking the nonadiabaticity with the population growth in the collective excitations of the dark state. Specifically, it was shown that a passage is adiabatic if the solution remains in a close proximity to the dark state. Itin and Watanabe [25] presented an improved adiabatic condition by applying methods of the classical Hamiltonian dynamics. The atom–molecule dark-state technique in the STIRAP was theoretically generalized to create more complex homonuclear or heteronuclear molecule trimers or tetramers [39–42].

An important issue is the instability and the adiabatic property of the dark state in such complex systems. For example, the dynamics of a nonlinear lambda system describing BEC of atoms and diatomic molecules was studied and a model of the dark state with collisional interactions was investigated [26, 27]. It was shown that nonlinear instabilities can be used for precise determination of the scattering lengths. On the other hand, the transfer of atoms to molecules via STIRAP is robust with respect to detunings, χ^3 nonlinearities and small asymmetries between the peak strengths of the two Raman lasers [27]. The complete conversion is destroyed by spatial effects unless the timescale of the coupling is much faster than the pulse duration. In addition, a set of robust and efficient techniques has been introduced [43] to coherently manipulate and transport neutral atoms based on three-level atom optics.

It is to be noted that the dynamics of an adiabatic sweep through a Feshbach resonance was studied [44] in a quantum gas of fermionic atoms. An interesting application of BEC is an atom diode with a directed motion of atoms [45]. Another example of BEC was presented in [46] where it was shown that the two-colour PA of fermionic atoms into bosonic molecules via a dark-state transition results in a significant reduction of the group velocity of the PA field. This is similar to the electromagnetically induced transparency (EIT) in atomic systems characterized by the three levels of the lambda type. In addition, the coupled nonlinear Schrödinger equations have been considered [47] to describe the atomic BECs interacting

with the molecular condensates through the STIRAP loaded in an external potential. The results have shown that there is a class of external potentials where the exact dark solutions can be formed. In [48], it was shown that it is possible to perform qubit rotations by STIRAP, and proposed a rotation procedure in which the resulting state corresponds to a rotation of the qubit, with the axis and angle of rotation determined uniquely by the parameters of the laser fields.

A relevant tool for studying the adiabaticity is the adiabatic fidelity. It indicates how far the current solution of the system from the dark state is. Meng *et al* have generalized the definition of fidelity for the nonlinear system [28]. They have studied the dynamics and adiabaticity of the population transfer for the atom–molecule three-level lambda system on a STIRAP. It was also discussed how to achieve higher adiabatic fidelity for the dark state through optimizing the external parameters of the STIRAP. In the subsequent paper [49], Meng *et al* have used the same definition of adiabatic fidelity in order to discuss the adiabatic evolution of the dark state in a nonlinear atom–trimer conversion due to a STIRAP. It is to be noted that Ivanov and Vitanov have recently proposed novel high-fidelity composite pulses for the most important single-qubit operations [50].

In this work, we analyse the problem of reducing the dimension (simplifying) in the linear/nonlinear three- and four-level models. This procedure is called the adiabatic reduction and its validity is closely related with the theory of adiabaticity discussed above. The exact three- or four-level system may be adiabatically reduced to a system with lower dimension. The question that arises is how many dynamic variables can be eliminated? In other words, what is the effective dimension of the system? The answer lies in the eigenvalues of the Jacobian computed at the dark state. The zero real parts of eigenvalues mean that in some directions the nearby solutions are behaving neutrally in respect to the dark state. The negative real parts in turn mean that some directions are stable, and the nearby solutions converge towards the dark state. Therefore, we conclude that the number of negative real parts dictates the number of variables that can be adiabatically eliminated (see e.g. [35]). On the other hand, the number of zero real parts yields the effective dimension of the system. Note that we find the non-zero eigenvalues analytically from quadratic characteristic equations.

One of the central issues in our work is the presence of dissipation in all the considered systems. The non-zero losses make the adiabatic reduction easier to implement since the term of losses acts as a 'controller' that attracts the nearby solutions towards the dark state. However, Vitanov and Stenholm have demonstrated that the losses cause also the decrease of transfer efficiency to the target state [8]. This decrease can be circumvented by higher pulse areas since the range of decay rates over which the transfer efficiency remains high has been found to be proportional to the squared pulse area (see (10) in [8]). In the subsequent developments, the effect of spontaneous emission on the population transfer efficiency in STIRAP was explored for the linear lambda [10, 11] and tripod [15] systems. In addition, Renzoni *et al* [51] have considered the coherent-population-trapping (CPT) phenomenon in a thermal sodium atomic beam. It was demonstrated that CPT may be realized on those open transitions with an efficiency decreasing with the amount of spontaneous emission towards external states. On the other hand, here we concentrate on the stability issues of the linear and nonlinear lambda and tripod systems with the losses.

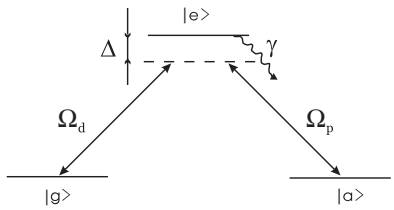

Figure 1. Three-level system coupled by two lasers. Ω_p and Ω_d are the Rabi frequencies for the pump and damp laser, Δ is the one photon detuning and γ is the loss rate.

The paper is organized as follows. In the next two sections, we shall consider the stability of the linear lambda and tripod systems with losses. In sections 4 and 5, the analysis is extended to the nonlinear lambda and tripod systems. In section 6, we discuss the role of the one-photon detuning followed by the conclusions in section 7.

2. The linear lambda system

In this section, we shall provide a summary on the STIRAP in the linear lambda system with losses studied in [8, 10, 11] followed by the stability analysis of the system. The three-level lambda system is shown in figure 1. The excited state $|e\rangle$ is coupled to two ground states $|a\rangle$ and $|g\rangle$ with the coupling strengths denoted as Ω_p and Ω_d to form a lambda scheme. The Hamiltonian of such a system reads

$$H = -\hbar(\Delta + i\gamma)|e\rangle\langle e| + \frac{\hbar}{2}[\Omega_p|a\rangle\langle e| + \Omega_d|g\rangle\langle e| + \text{h.c.}]. \quad (1)$$

Note that in this Hamiltonian besides the real-valued one-photon detuning Δ there is the imaginary term γ representing the losses. Denoting the amplitudes of the three-level state as ψ_e, ψ_a and ψ_g respectively, we obtain the Schrödinger equation:

$$i\dot{\psi}_a = \Omega_p\psi_e, \quad (2)$$

$$i\dot{\psi}_e = -(\Delta + i\gamma)\psi_e + \Omega_p\psi_a + \Omega_d\psi_g, \quad (3)$$

$$i\dot{\psi}_g = \Omega_d\psi_e. \quad (4)$$

The normalization reads

$$|\psi_a(t)|^2 + |\psi_g(t)|^2 + |\psi_e(t)|^2 \leqslant 1, \quad (5)$$

where equality holds for initial time. Because of losses ($\gamma > 0$), the total normalization will be slightly reduced (for $t > 0$) during the transfer of population through the excited level. This property of the total population is assumed throughout the paper.

We take the laser pulses to be Gaussian:

$$\Omega_d = \Omega_0 \exp\left[-\frac{(t - t_d)^2}{T^2}\right], \quad (6)$$

$$\Omega_p = \Omega_0 \exp\left[-\frac{(t - t_p)^2}{T^2}\right]. \quad (7)$$

Here, the pulses are centred at t_d and t_p, respectively, T is their width and Ω_0 is their amplitude.

The third-order system ((2)–(4)) may be rewritten in a matrix form

$$\dot{\mathbf{\Psi}} = -\mathrm{i}H\mathbf{\Psi} \equiv A\mathbf{\Psi}, \tag{8}$$

where $\mathbf{\Psi} = [\psi_a, \psi_e, \psi_g]^T$ is the vector of the state of the system, and

$$H = \begin{pmatrix} 0 & \Omega_p & 0 \\ \Omega_p & -(\Delta + \mathrm{i}\gamma) & \Omega_d \\ 0 & \Omega_d & 0 \end{pmatrix} \tag{9}$$

is the corresponding Hamiltonian. The matrix $A \equiv -\mathrm{i}H$ is the Jacobian of the system. If the Hamiltonian possesses eigenvalues ω, then the eigenvalues of the Jacobian are defined by $\lambda = -\mathrm{i}\omega$. Note that the real parts of λ determine the stability of the fixed point at the origin.

We now find these eigenvalues, more specifically their real parts. The eigenvalues of Hamiltonian satisfy the characteristic equation

$$\det ||H - I\omega|| = 0, \tag{10}$$

with I denoting the unit matrix. Expanding the corresponding third-order determinant one finds that one eigenvalue is always zero:

$$\omega_1 = 0. \tag{11}$$

The other two eigenvalues satisfy the quadratic equation:

$$\omega^2 + (\Delta + \mathrm{i}\gamma)\omega - \left(\Omega_d^2 + \Omega_p^2\right) = 0. \tag{12}$$

Thus, the two eigenvalues satisfy

$$\omega_2 + \omega_3 = -[\Delta + \mathrm{i}\gamma], \tag{13}$$

$$\omega_2\omega_3 = -\left[\Omega_d^2 + \Omega_p^2\right]. \tag{14}$$

Assuming $\Delta = 0$, the solutions of (12) read

$$\omega_{2,3} = \left\{-\mathrm{i}\gamma \pm \left[-\gamma^2 + 4\left(\Omega_d^2 + \Omega_p^2\right)\right]^{1/2}\right\}/2. \tag{15}$$

For $t \to \pm\infty$, the Rabi frequencies go to zero, and it follows from (13) and (14) that $\omega_2 = 0$, $\omega_3 = -\mathrm{i}\gamma$. Recalling (11), we can write

$$\lambda_{1,2} = 0, \quad \lambda_3 = -\gamma, \tag{16}$$

or $\mathrm{Re}(\lambda_{1,2}) = 0$ and $\mathrm{Re}(\lambda_3) = -\gamma$ for $t \to \pm\infty$.

For finite times, there is a region where the Rabi frequencies are large enough, so that the discriminant is positive in (15): $D \equiv -\gamma^2 + 4(\Omega_d^2 + \Omega_p^2) > 0$. Such a situation occurs in a certain interval $t_1 < t < t_2$, and from (15) we obtain

$$\omega_{2,3} = -\mathrm{i}\gamma/2 \pm \sqrt{D}/2, \tag{17}$$

$$\lambda_{2,3} = -\gamma/2 \mp \mathrm{i}\sqrt{D}/2. \tag{18}$$

The first eigenvalue is $\lambda_1 = \omega_1 = 0$. The boundaries t_1 and t_2 are the solutions of $D(t) = 0$ with respect to time.

Hence, in the interval $t_1 < t < t_2$, the real parts are $\mathrm{Re}(\lambda_1) = 0$, $\mathrm{Re}(\lambda_{2,3}) = -\gamma/2$.

We may adiabatically reduce the dimension of this system, but we first transform its variables. We change the bare variables ψ_a and ψ_g to the bright ψ_B and dark ψ_D one:

$$\psi_B = (\Omega_p\psi_a + \Omega_d\psi_g)/\Omega, \tag{19}$$

$$\psi_D = (\Omega_d\psi_a - \Omega_p\psi_g)/\Omega, \tag{20}$$

where

$$\Omega = \left(\Omega_p^2 + \Omega_d^2\right)^{1/2}. \tag{21}$$

Denoting $\xi_p = \Omega_p/\Omega$, $\xi_d = \Omega_d/\Omega$, and performing some operations, we obtain the following equations for the new variables:

$$\mathrm{i}\dot{\psi}_B = \alpha\psi_D + T\Omega\psi_e, \tag{22}$$

$$\mathrm{i}\dot{\psi}_e = -T(\Delta + \mathrm{i}\gamma)\psi_e + T\Omega\psi_B, \tag{23}$$

$$\mathrm{i}\dot{\psi}_D = \alpha^*\psi_B, \tag{24}$$

where we have made the time dimensionless by substituting $t/T \to t$. Here, $\alpha = \mathrm{i}(\dot{\xi}_p\xi_d - \dot{\xi}_d\xi_p)$ is a dimensionless parameter in which derivatives $\dot{\xi}_p$ and $\dot{\xi}_d$ are taken with respect to dimensionless time.

We now adiabatically eliminate the amplitude ψ_e by setting $\dot{\psi}_e = 0$. From (23), we obtain

$$\psi_e = \frac{\Omega}{\Delta + \mathrm{i}\gamma}\psi_B. \tag{25}$$

Inserting this result in (22) and (24), we obtain

$$\mathrm{i}\dot{\psi}_B = \alpha\psi_D + \frac{T\Omega^2}{\Delta + \mathrm{i}\gamma}\psi_B, \tag{26}$$

$$\mathrm{i}\dot{\psi}_D = \alpha^*\psi_B. \tag{27}$$

We solve this system to find the dynamics of ψ_B and ψ_D, and from (25) we find the dynamics of ψ_e.

The system ((26), (27)) may also be adiabatically reduced. We now set $\dot{\psi}_B = 0$ and solve (26) for ψ_B:

$$\psi_B = -\frac{\alpha(\Delta + \mathrm{i}\gamma)}{T\Omega^2}\psi_D. \tag{28}$$

Inserting this result in (27), we obtain a first-order dynamic system:

$$\mathrm{i}\dot{\psi}_D = -\frac{|\alpha|^2(\Delta + \mathrm{i}\gamma)}{T\Omega^2}\psi_D. \tag{29}$$

The Hamiltonian for the 2D reduced system ((26), (27)) reads

$$H_{2D} = \begin{pmatrix} \dfrac{T\Omega^2}{\Delta + \mathrm{i}\gamma} & \alpha \\ \alpha^* & 0 \end{pmatrix}. \tag{30}$$

Solving the characteristic equation for this Hamiltonian, and assuming $\Delta = 0$, one obtains two eigenvalues:

$$\omega_{1,2} = \frac{\mathrm{i}}{2}\left[-\frac{T\Omega^2}{\gamma} \pm \left(\frac{T^2\Omega^4}{\gamma^2} - 4|\alpha|^2\right)^{1/2}\right], \tag{31}$$

$$\lambda_{1,2} = \frac{1}{2}\left[-\frac{T\Omega^2}{\gamma} \pm \left(\frac{T^2\Omega^4}{\gamma^2} - 4|\alpha|^2\right)^{1/2}\right]. \tag{32}$$

Here, $\lambda_{1,2}$ are the eigenvalues of the corresponding Jacobian defined as $A_{2D} \equiv -\mathrm{i}H_{2D}$. There are two regimes of evolution of the eigenvalues corresponding to $D_2 < 0$ and $D_2 > 0$, where $D_2 = \frac{T^2\Omega^4}{\gamma^2} - 4|\alpha|^2$ is the discriminant in (31) and (32).

Hence, we have the eigenvalues for all three versions of the linear lambda system. For the exact 3D system, they are given by $\lambda_1 = \omega_1 = 0$ and (17) and (18). For the reduced

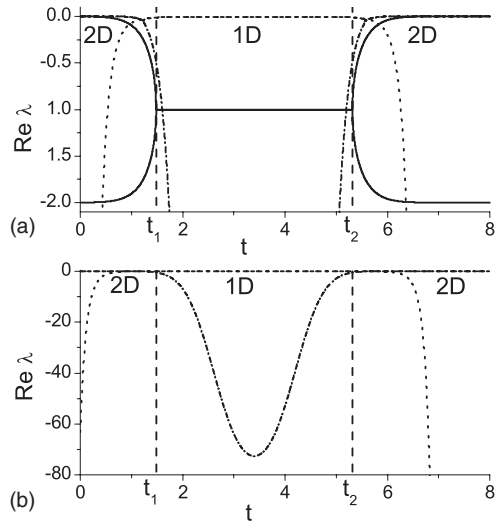

Figure 2. (a) Dynamics of real parts of eigenvalues of the Jacobian for linear lambda system, computed for all three cases (3D, 2D and 1D) by (17), (18), (31), (32) and (33), respectively. The dashed vertical lines set the boundaries for the 1D and 2D processes. Here, $t_1 = 1.49$ and $t_2 = 5.32$. The solid lines are the real parts for the 3D, the short-dash-dotted and short-dashed line correspond to the 2D case, and the dotted line is the real part for the 1D reduced system; (b) the dynamics of real parts for the 2D and 1D cases in an extended vertical scale. The lines are chosen in the same way as in (a). The parameters are as follows: $\Delta = 0$, $\gamma = 2.0$, $\Omega_0 = 10.0$, $t_p = 3.8$, $t_d = 3.0$ and $T = 1.0$.

2D system, they read (31) and (32). Finally, a trivial single eigenvalue for the 1D system follows from (29):

$$\lambda_1 = -\mathrm{i}\omega_1 = -\frac{|\alpha|^2\gamma}{T\Omega^2}. \tag{33}$$

In figure 2, we show the dynamics of the real parts of eigenvalues for all three cases.

As the solid lines in figure 2(a) show, for $t < t_1$ and $t > t_2$ there are two different non-zero branches for the 3D case: the upper branch determines the slow decay of the bright state, whereas the lower branch causes the fast decay of the excited one. Therefore, we may eliminate the excited state, and cannot do this with the bright one. In the middle of the process, where $t_1 < t < t_2$, both branches become degenerate with the real part of eigenvalues equal to $-\gamma/2$. We thus may reduce both states, excited and bright. During the whole evolution, one real part remains exactly zero showing that the dark state does not experience any losses. This fact indicates that the process is adiabatic.

The short-dash-dotted and short-dashed lines show the dynamics of two real parts for the 2D reduced system. Although the time moments $[(\tilde{t}_1, \tilde{t}_2) = (1.24, 5.56)]$ at which the discriminant D_2 is zero differ from the times $[(t_1, t_2) = (1.49, 5.32)]$, where the discriminant D goes to zero, these differences are small compared to the interval $(t_2 - t_1)$. In the time intervals of $t < t_1$ and $t > t_2$, both branches are close to zero indicating that neither the bright nor dark state may be eliminated. The process here again is 2D. In contrast, in the range of time, where $t_1 < t < t_2$, the decay rate of the bright state is very large compared to that of the dark state. It is well seen in figure 2(b). Therefore, the process is again 1D as for the exact case.

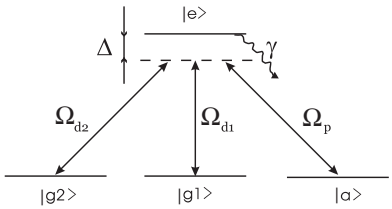

Figure 3. Four-level system coupled with three lasers. Ω_p, Ω_{d1} and Ω_{d2} are the Rabi frequencies for the pump, and damp lasers, Δ is the one-photon detuning, and γ is the loss rate.

And lastly, the dotted line shows the dynamics of the real part for the 1D reduced system. One may clearly see that for $t < t_1$ and $t > t_2$, the decay of the dark state is rapid compared to that for $t_1 < t < t_2$. The fastness of decay for $t < t_1$ and $t > t_2$ is seen expressively in figure 2(b). This leads to the conclusion that the 1D reduced system is appropriate only in the time interval of $t_1 < t < t_2$.

Exactly as for the 3D system, the evolution of the system in the 2D (1D) approximations is adiabatic for the whole time of integration (in the time interval $t_1 < t < t_2$) since for both cases the decay rate of the dark state is very small compared with that of the bright state.

3. The linear tripod

The STIRAP process in the linear tripod scheme without dissipation was first considered by Unanyan *et al* [13, 14]. Here, we outline this scheme in which the dissipation is also included. Afterwards, we perform the linear analysis of this system.

Consider the four-level system schematically shown in figure 3. The excited state $|\mathrm{e}\rangle$ is coupled to three ground states $|\mathrm{a}\rangle$, $|\mathrm{g1}\rangle$ and $|\mathrm{g2}\rangle$ with the coupling strengths denoted as Ω_p, Ω_{d1} and Ω_{d2}, respectively. Here, p stands for pump and d stands for the damp. The four-level Hamiltonian reads

$$H = -\hbar(\Delta + \mathrm{i}\gamma)|\mathrm{e}\rangle\langle\mathrm{e}| + \frac{\hbar}{2}[\Omega_p|\mathrm{a}\rangle\langle\mathrm{e}| + \Omega_{d1}|\mathrm{g1}\rangle\langle\mathrm{e}| + \Omega_{d2}|\mathrm{g2}\rangle\langle\mathrm{e}| + \mathrm{h.c.}]. \tag{34}$$

Denoting the amplitudes as ψ_e, ψ_a, ψ_{g1} and ψ_{g2}, the Schrödinger equation reads

$$\mathrm{i}\dot{\psi}_a = \Omega_p\psi_e, \tag{35}$$

$$\mathrm{i}\dot{\psi}_e = -(\Delta + \mathrm{i}\gamma)\psi_e + \Omega_p\psi_a + \Omega_{d1}\psi_{g1} + \Omega_{d2}\psi_{g2}, \tag{36}$$

$$\mathrm{i}\dot{\psi}_{g1} = \Omega_{d1}\psi_e, \tag{37}$$

$$\mathrm{i}\dot{\psi}_{g2} = \Omega_{d2}\psi_e. \tag{38}$$

The normalization is given by

$$|\psi_a(t)|^2 + |\psi_{g1}(t)|^2 + |\psi_{g2}(t)|^2 + |\psi_e(t)|^2 \leqslant 1, \tag{39}$$

where equality holds for initial time.

The Rabi frequencies are given by

$$\Omega_p = \Omega_0 \exp\left[-\frac{(t - t_p)^2}{T^2}\right], \tag{40}$$

$$\Omega_{d1} = K_1\Omega_0 \exp\left[-\frac{(t - t_{d1})^2}{T^2}\right], \tag{41}$$

$$\Omega_{d2} = K_2\Omega_0 \exp\left[-\frac{(t-t_{d2})^2}{T^2}\right]. \quad (42)$$

Here, the pulses are centred at t_p, t_{d1} and t_{d2}, respectively. T is the width of the pulses, K_1 and K_2 determine the amplitudes for the damp pulses and Ω_0 is the amplitude of the pump pulse.

The system ((35)–(38)) can be written in the form of (8) with the state vector $\mathbf{\Psi} = [\psi_a, \psi_e, \psi_{g1}, \psi_{g2}]^T$ and Hamiltonian

$$H = \begin{pmatrix} 0 & \Omega_p & 0 & 0 \\ \Omega_p & -(\Delta + i\gamma) & \Omega_{d1} & \Omega_{d2} \\ 0 & \Omega_{d1} & 0 & 0 \\ 0 & \Omega_{d2} & 0 & 0 \end{pmatrix}. \quad (43)$$

The matrix $A \equiv -iH$ is again the Jacobian of the system. Here, the relation $\lambda = -i\omega$ holds. Solving the eigenvalues problem (10) for the linear tripod, we obtain two zero eigenvalues,

$$\omega_{1,2} = 0. \quad (44)$$

The other two eigenvalues can be found from quadratic equation

$$\omega^2 + (\Delta + i\gamma)\omega - \left(\Omega_{d1}^2 + \Omega_{d2}^2 + \Omega_p^2\right) = 0. \quad (45)$$

The eigenvalues $\omega_{3,4}$ must satisfy

$$\omega_3 + \omega_4 = -(\Delta + i\gamma), \quad (46)$$

$$\omega_3\omega_4 = -\left(\Omega_{d1}^2 + \Omega_{d2}^2 + \Omega_p^2\right). \quad (47)$$

We again assume that $\Delta = 0$, thus obtaining the following solutions:

$$\omega_{3,4} = \left\{-i\gamma \pm \left[-\gamma^2 + 4\left(\Omega_{d1}^2 + \Omega_{d2}^2 + \Omega_p^2\right)\right]^{1/2}\right\}/2. \quad (48)$$

(see also (7) in [14]). The Rabi frequencies are chosen in the form of Gaussian pulses. For $t \to \pm\infty$, the Rabi frequencies tend to zero, and from (46) and (47) it follows that $\omega_3 = 0$, $\omega_4 = -i\gamma$. Hence, for $t \to \pm\infty$, we have

$$\lambda_{1,2,3} = 0, \quad \lambda_4 = -\gamma. \quad (49)$$

However, between these two infinite times there is a region where the Rabi frequencies are large enough and the discriminant in (48) is positive [$D \equiv -\gamma^2 + 4(\Omega_{d1}^2 + \Omega_{d2}^2 + \Omega_p^2) > 0$]. Such a situation takes place in the interval $t_1 < t < t_2$, and from (48) we obtain

$$\omega_{3,4} = -i\gamma/2 \pm \sqrt{D}/2, \quad (50)$$

$$\lambda_{3,4} = -\gamma/2 \mp i\sqrt{D}/2. \quad (51)$$

The first two eigenvalues are $\lambda_{1,2} = \omega_{1,2} = 0$. The boundaries t_1 and t_2 are defined in the same way as in section 3.

Hence, in the interval $t_1 < t < t_2$, the real parts are $\mathrm{Re}(\lambda_{1,2}) = 0$, $\mathrm{Re}(\lambda_{3,4}) = -\gamma/2$.

Exactly as in the previous section, we first transform the variables from the bare states to one bright and two dark states:

$$(\psi_a, \psi_e, \psi_{g1}, \psi_{g2}) \to (\psi_B, \psi_e, \psi_{D1}, \psi_{D2}). \quad (52)$$

Parametrizing the Rabi frequencies as

$$\Omega_{d2} = \Omega \sin(\phi), \quad (53)$$

$$\Omega_p = \Omega \cos(\phi)\sin(\Theta), \quad (54)$$

$$\Omega_{d1} = \Omega \cos(\phi)\cos(\Theta), \quad (55)$$

we may write down the amplitudes of one bright and two dark states:

$$\psi_B = \cos(\phi)\sin(\Theta)\psi_a + \cos(\phi)\cos(\Theta)\psi_{g1} + \sin(\phi)\psi_{g2}, \quad (56)$$

$$\psi_{D1} = \cos(\Theta)\psi_a - \sin(\Theta)\psi_{g1}, \quad (57)$$

$$\psi_{D2} = \sin(\phi)\sin(\Theta)\psi_a + \sin(\phi)\cos(\Theta)\psi_{g1} - \cos(\phi)\psi_{g2}. \quad (58)$$

After renormalizing the time ($t/T \to t$) and some rearrangements, we derive the following dynamic system for these variables:

$$i\frac{d}{dt}\begin{pmatrix}\psi_B \\ \psi_e \\ \psi_{D1} \\ \psi_{D2}\end{pmatrix} = \begin{pmatrix} 0 & T\Omega & \alpha_{13} & \alpha_{14} \\ T\Omega & -T(\Delta + i\gamma) & 0 & 0 \\ \alpha_{13}^* & 0 & 0 & \alpha_{34} \\ \alpha_{14}^* & 0 & \alpha_{34}^* & 0 \end{pmatrix}\begin{pmatrix}\psi_B \\ \psi_e \\ \psi_{D1} \\ \psi_{D2}\end{pmatrix}. \quad (59)$$

Here,

$$\alpha_{13} = i(\dot{\xi}_{11}\xi_{31} + \dot{\xi}_{13}\xi_{33}), \quad (60)$$

$$\alpha_{14} = i(\dot{\xi}_{11}\xi_{41} + \dot{\xi}_{13}\xi_{43} + \dot{\xi}_{14}\xi_{44}), \quad (61)$$

$$\alpha_{34} = i(\dot{\xi}_{31}\xi_{41} + \dot{\xi}_{33}\xi_{43}), \quad (62)$$

and the coefficients ξ_{ij} are defined by the matrix

$$||\xi_{ij}|| = \begin{pmatrix} \cos(\phi)\sin(\Theta) & 0 & \cos(\phi)\cos(\Theta) & \sin(\phi) \\ 0 & 1 & 0 & 0 \\ \cos(\Theta) & 0 & -\sin(\Theta) & 0 \\ \sin(\phi)\sin(\Theta) & 0 & \sin(\phi)\cos(\Theta) & -\cos(\phi) \end{pmatrix}. \quad (63)$$

Note that this matrix realizes the transformation (52) (see also (56)–(58)).

We now reduce the dimension of the system (59) in two steps. For the first step, we eliminate the excited state by setting

$$\dot{\psi}_e = 0. \quad (64)$$

Solving the equation

$$\Omega\psi_B - (\Delta + i\gamma)\psi_e = 0, \quad (65)$$

(see the second row in (59)) for ψ_e, we obtain

$$\psi_e = \frac{\Omega}{\Delta + i\gamma}\psi_B. \quad (66)$$

Inserting this result in (59), we obtain the following three-dimensional dynamic system:

$$i\frac{d}{dt}\begin{pmatrix}\psi_B \\ \psi_{D1} \\ \psi_{D2}\end{pmatrix} = \begin{pmatrix} \frac{T\Omega^2}{\Delta + i\gamma} & \alpha_{13} & \alpha_{14} \\ \alpha_{13}^* & 0 & \alpha_{34} \\ \alpha_{14}^* & \alpha_{34}^* & 0 \end{pmatrix}\begin{pmatrix}\psi_B \\ \psi_{D1} \\ \psi_{D2}\end{pmatrix}. \quad (67)$$

We can solve this system to find the evolution of $\psi_B, \psi_{D1}, \psi_{D2}$, and to determine the dynamics of the excited state using (66).

For the second step, we eliminate the bright state, i.e. we set

$$\dot{\psi}_B = 0, \quad (68)$$

in (67). After solving the equation

$$\frac{T\Omega^2}{\Delta + \mathrm{i}\gamma}\psi_{\mathrm{B}} + \alpha_{13}\psi_{\mathrm{D1}} + \alpha_{14}\psi_{\mathrm{D2}} = 0, \tag{69}$$

for ψ_{B} (see the first row in (67)), we find

$$\psi_{\mathrm{B}} = -\frac{\Delta + \mathrm{i}\gamma}{T\Omega^2}(\alpha_{13}\psi_{\mathrm{D1}} + \alpha_{14}\psi_{\mathrm{D2}}). \tag{70}$$

Inserting this result in (67), we obtain the following second-order system:

$$\mathrm{i}\frac{\mathrm{d}}{\mathrm{d}t}\begin{pmatrix}\psi_{\mathrm{D1}}\\ \psi_{\mathrm{D2}}\end{pmatrix} = H_2\begin{pmatrix}\psi_{\mathrm{D1}}\\ \psi_{\mathrm{D2}}\end{pmatrix}. \tag{71}$$

The matrix of this system may be split into two parts:

$$H_2 = H_2^{(0)} + \frac{\Delta + \mathrm{i}\gamma}{T\Omega^2}H_2^{(1)}, \tag{72}$$

where

$$H_2^{(0)} = \begin{pmatrix}0 & \alpha_{34}\\ \alpha_{34}^* & 0\end{pmatrix}, \tag{73}$$

and

$$H_2^{(1)} = -\begin{pmatrix}|\alpha_{13}|^2 & \alpha_{13}^*\alpha_{14}\\ \alpha_{14}^*\alpha_{13} & |\alpha_{14}|^2\end{pmatrix}. \tag{74}$$

When Ω^2 is relatively large, one can neglect the influence of $H_2^{(1)}$ and write approximately $H_2 \simeq H_2^{(0)}$. Thus, one arrives at a simple second-order system

$$\mathrm{i}\frac{\mathrm{d}}{\mathrm{d}t}\begin{pmatrix}\psi_{\mathrm{D1}}\\ \psi_{\mathrm{D2}}\end{pmatrix} = \begin{pmatrix}0 & \alpha_{34}\\ \alpha_{34}^* & 0\end{pmatrix}\begin{pmatrix}\psi_{\mathrm{D1}}\\ \psi_{\mathrm{D2}}\end{pmatrix}, \tag{75}$$

which is equivalent to (27) of [13]. However, this system is not an adiabatically reduced version of the system ((35)–(38)). Actually, it determines the solution moving exactly on the dark-state manifold comprising the two degenerate states $|D1\rangle$ and $|D2\rangle$. (This statement can be confirmed by applying the approach of [32].) Comparing (72) with the corresponding result for the linear lambda system (29), we note that both Hamiltonians contain the characteristic timescale T (the pulse width) in the denominators. In the case of (72), this timescale is involved only with the correct Hamiltonian $H_2^{(1)}$, and it is absent in $H_2^{(0)}$ since it corresponds to a zero on the rhs of (29). The correction $H_2^{(1)}$ in (72) thus corresponds to the rhs of (29).

Figure 4 shows the dynamics of the real parts of the eigenvalues of the Jacobians for various dimensions. In figure 4(a), the solid lines correspond to the exact 4D case. For $t < t_1$ and $t > t_2$, the lower branch, for which $\mathrm{Re}\,\lambda \simeq -\gamma$, causes the decay of the excited state. The upper branch describing the decay rate for the bright state is small compared to the decay rate of the excited state in these time intervals indicating that the excited state may be adiabatically eliminated, whereas the bright state must be left. In the middle of the passage ($t_1 < t < t_2$), the decay rates of the excited and bright states become degenerate and equal to $-\gamma/2$, thus enabling us to eliminate them both. The eigenvalues for both the dark states remain zeros for the whole evolution of the system demonstrating that the process is adiabatic since the degenerate dark state does not loose its population.

The dash-dotted line in figure 4 displays the dynamics of the decay rate for the bright state in the 3D system. In figure 4(a), it falls down (grows up) just after t_1 (just before t_2). In figure 4(b), the same dynamics is shown in an extended vertical scale. From both figures 4(a) and (b), one may conclude that in the 3D reduced system the bright state may be eliminated for $t_1 < t < t_2$, and it should be preserved for $t < t_1$ and $t > t_2$, since its decay rate in the latter case is much less than in the former one. The two eigenvalues corresponding to degenerate dark states remain exactly (or almost) zero for the 3D system. They are small compared with the decay rate of the bright state. Therefore these states may not be eliminated for the whole time of evolution.

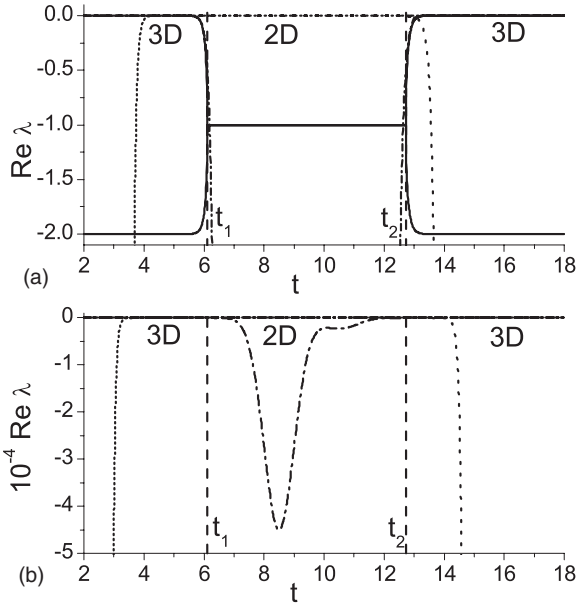

Figure 4. (a) Dynamics of real parts of eigenvalues of the Jacobian for a linear tripod, computed for all three cases (4D, 3D and 2D) by (48) and (44), and from (67) and (72). The dashed vertical lines set the boundaries for the 2D and 3D processes. Here, $t_1 = 6.12$ and $t_2 = 12.73$. The solid lines are the real parts for the 4D, the short-dash-dotted and short-dashed line correspond to the 3D case, and the dotted and the short-dotted lines are the real parts for the 2D reduced system; (b) the dynamics of real parts for the 3D and 2D cases in an extended vertical scale. The lines are chosen in the same way as in (a). The parameters are as follows: $\Delta = 0$, $\gamma = 2.0$, $\Omega_0 = 60.0$, $t_{\mathrm{p}} = 10.7$, $t_{\mathrm{d1}} = 10.0$, $t_{\mathrm{d2}} = 8.5$, $K_1 = 0.75$, $K_2 = 5.0$ and $T = 1.0$.

The dotted and short-dotted lines in figure 4 show the dynamics of the real parts for the 2D reduced system. One of them grows rapidly before t_1 and converges to zero, whereas the other one is first zero and then decays rapidly after t_2. Such a situation suggests that the range of applicability of the 2D system should be wider than the time interval $t_1 < t < t_2$ since the two degenerate dark states survive (do not decay) when the decay rate is relatively small. However, such a conclusion would be true if the whole population among the degenerate states were distributed at the end of the rapid growth of the first real part. But if the bright state had some initial population, it could not be neglected since its real part is close to zero before t_1 and after t_2.

We should also note here that for the 2D reduced system, the decay rate for the second dark state grows rapidly from negative values to zero (the decay rate for the first dark state decreases rapidly from zero to negative values) in the time intervals $t < 2.0$ ($t > 18.0$), i.e. outside of the figure 4. But

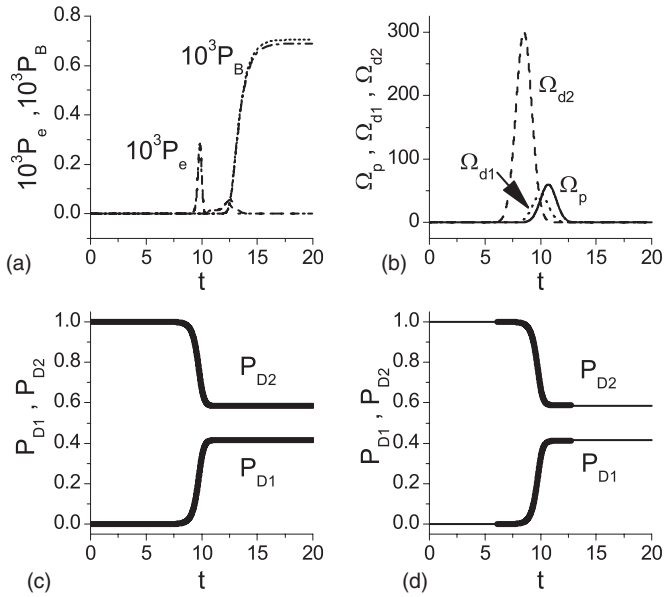

Figure 5. (a) The dynamics of populations 10^3P_e, 10^3P_B that are computed from (35) to (38) (dashed/dash-dotted lines), and from (67) and (66) (dotted/short–dotted lines); (b) the dynamics of Gaussian pulses computed by (40)–(42); (c) and (d) the dynamics of populations of dark states computed in (c) by (35)–(38) (thin solid line) and by (67) (thick solid line); in (d) the thin solid line represents again the exact solutions of (35)–(38) and the thick solid line is obtained using the approximation from (71) computed in the range of $t_1 < t < t_2$. The parameters are the same as in figure 4. The initial conditions are $\psi_a(0) = 1$, $\psi_{g1}(0) = \psi_{g2}(0) = \psi_e(0) = 0$.

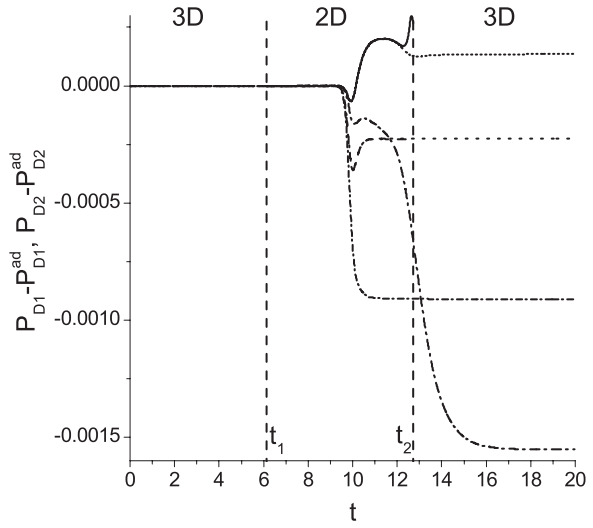

Figure 6. The differences between the exact and approximated degenerate dark states; the short-dotted and dotted lines show the differences of $P_{D1} - P_{D1}^{ad}$ and $P_{D2} - P_{D2}^{ad}$ for the 3D system (67), respectively; the dash-dotted and short-dash-dotted lines display the corresponding differences for P_{D1} and P_{D2} for the 2D system (75), respectively; the solid and dashed lines show the differences for P_{D1} and P_{D2} for the adiabatically reduced system (71), respectively (integrated only in the range of $t_1 < t < t_2$). The vertical dashed lines set the boundaries for the 3D and 2D processes. The parameters and initial conditions are the same as in figure 5.

we do not need to take these events into account since we are interested in the time interval where both decay rates are close to zero. This interval is determined by the growing (decreasing) decay rates which are plotted in figure 4.

Exactly as in the previous section, we here can also conclude that the adiabaticity is preserved also for reduced systems, since for the 3D (2D) approximations the dark-state manifold does not lose its population for the whole time of evolution (in the time interval that is wider than $t_1 < t < t_2$).

Figure 5 displays the results of numerical computations. In figure 5(a), we have presented the dynamics of populations of the bright (dashed and dotted lines), and excited (dash-dotted and short-dotted lines) states. The dashed and dotted lines correspond to solutions of exact equations (35)–(38). The dash-dotted and short–dotted lines are obtained from (67) (the bright state), and from (66) (the excited state). One can see that the populations of these states remain relatively small ($P_e, P_B \simeq 10^{-3}$). In figure 5(b), the dynamics of coupling strengths is shown. Figures 5(c) and (d) display the dynamics of populations of the degenerate dark states. Figure 5(c) presents the solutions of exact (35)–(38) (thin solid line) and that of adiabatically reduced system (67) (thick solid line). The exact and approximate solutions are in good quantitative agreement (we do not distinguish them in the present graph). Both systems were integrated in the whole time range ($t \in [0.0, 20.0]$). In figure 5(d), we compare the dynamics for exact (35)–(38) (thin solid line) with those of adiabatically simplified (71) (thick solid line).

In figure 6, we compare the exactness of various approximations for the nonlinear tripod. We see that the system (75) is in a good quantitative agreement with the exact system, but it is worse than (67) in the range $t > t_1$. Whereas the 2D approximation (71) coincides with the solution of (67) in the interval $t_1 < t < t_2$ almost identically. At the end of this interval, just before t_2, the solution of (71) slightly deviates from that of (67). This is due to the fact that the magnitude of element $\frac{\gamma}{T\Omega^2}|\alpha_{13}|^2$ contributed by the matrix $H_2^{(1)}$ in (72) becomes large compared with the magnitude of the element α_{34} of the matrix $H_2^{(0)}$, (73). The remaining elements of $H_2^{(1)}$ are much less than $|\alpha_{13}|^2$ just before t_2.

We should also note that in figure 6, the solution of a 'non-exact' 2D system (73) coincides almost identically with the exact 4D solution in the range of $t < t_1$. However, such a situation takes place when the initial conditions are very close to the dark state. If we pushed them away from the dark state, the result of (73) would become worse than that of the 3D system (67) (not shown here). The system thus remains effectively 3D in the range of $t < t_1$.

Similarly, it can be numerically verified that the solution of (71) is not worse than that of (67) just before t_2 if one pushes the initial conditions further away from the dark-state manifold. Therefore, the system remains 2D in the whole interval $t_1 < t < t_2$.

4. The nonlinear lambda system

The three-level nonlinear Hamiltonian for the nonlinear lambda system (see the figure 1) reads

$$\hat{H} = -\hbar(\Delta + i\gamma)\hat{\psi}_e^\dagger\hat{\psi}_e + \frac{\hbar}{2}\left(\Omega_p\hat{\psi}_e^\dagger\hat{\psi}_a\hat{\psi}_a + \Omega_d\hat{\psi}_e^\dagger\hat{\psi}_g + \text{h.c.}\right). \tag{76}$$

Here, $\hat{\psi}_\alpha$, $\hat{\psi}_\alpha^\dagger$ ($\alpha = \mathrm{a}, \mathrm{e}, \mathrm{g}$) are the bosonic annihilation and creation operators for state α, respectively. When the number of particles is much larger than unity, the boson operators are replaced by c numbers ψ_α, ψ_α^* (the meanfield treatment [29, 37]) which obey the following Heisenberg equations:

$$\mathrm{i}\dot{\psi}_\mathrm{a} = \Omega_\mathrm{p}\psi_\mathrm{a}^*\psi_\mathrm{e}, \tag{77}$$

$$\mathrm{i}\dot{\psi}_\mathrm{e} = -(\Delta + \mathrm{i}\gamma)\psi_\mathrm{e} + \tfrac{1}{2}\Omega_\mathrm{p}\psi_\mathrm{a}^2 + \tfrac{1}{2}\Omega_\mathrm{d}\psi_\mathrm{g}, \tag{78}$$

$$\mathrm{i}\dot{\psi}_\mathrm{g} = \tfrac{1}{2}\Omega_\mathrm{d}\psi_\mathrm{e}. \tag{79}$$

The normalization reads

$$|\psi_\mathrm{a}(t)|^2 + 2[|\psi_\mathrm{g}(t)|^2 + |\psi_\mathrm{e}(t)|^2] \leqslant 1, \tag{80}$$

where the equality holds for the initial time.

The nonlinearity enters here in the coupling induced by the pump field: it couples a particle in the state e with a pair of particles in the state a. Such a nonlinear coupling is encountered in the second harmonic generation in nonlinear optics (where a represents the fundamental photon and e its second harmonics), as well as in the PA of atoms into diatomic molecules [20, 21, 29, 37], where a represents an atomic state, while e and g are excited and ground diatomic molecular states, respectively.

As for the linear lambda system, we take the Gaussian pulses given by (6) and (7).

Similar as in two previous sections, we here define the state vector $\boldsymbol{\Psi} = [\psi_\mathrm{a}, \psi_\mathrm{e}, \psi_\mathrm{g}]^T$. The dynamic system ((77)–(79)) can be rewritten in the vector form:

$$\mathrm{i}\frac{\mathrm{d}}{\mathrm{d}t}\boldsymbol{\Psi} = \boldsymbol{f}(\boldsymbol{\Psi}), \tag{81}$$

where $\boldsymbol{f}$ is the vector of (generally) nonlinear functions on the rhs of the system ((77)–(79)). The steady-state solution $\boldsymbol{\Psi}_0(t)$ of this system represents the dark state which is obtained by solving

$$\boldsymbol{f}(\boldsymbol{\Psi}_0) = \boldsymbol{0}. \tag{82}$$

For the nonlinear lambda system ((77)–(79)), the dark state reads [29, 37]

$$\psi_\mathrm{a}^0 = \left[\frac{2\Omega_\mathrm{d}}{\Omega_\mathrm{d} + \Omega_\mathrm{eff}}\right]^{1/2}, \quad \psi_\mathrm{e}^0 = 0, \quad \psi_\mathrm{g}^0 = -\frac{2\Omega_\mathrm{p}}{\Omega_\mathrm{d} + \Omega_\mathrm{eff}}, \tag{83}$$

with $\Omega_\mathrm{eff} = \left(\Omega_\mathrm{d}^2 + 8\Omega_\mathrm{p}^2\right)^{1/2}$.

If the solution remains in this state for the whole time, the adiabatic passage from the initially occupied state a to the target state g takes place provided the Gaussian pulses $\Omega_\mathrm{d}(t)$, $\Omega_\mathrm{p}(t)$ arrive in a counter-intuitive sequence.

We are now interested in the linear stability of the dark state (83). To this end, we suppose that the solution of (81) evolves in the close neighbourhood of the dark state $\boldsymbol{\Psi}_0$, i.e. we express it as a sum

$$\boldsymbol{\Psi}(t) = \boldsymbol{\Psi}_0(t) + \delta\boldsymbol{\Psi}(t), \tag{84}$$

where $\delta\boldsymbol{\Psi}(t)$ is a deviation of the current solution from the dark state. Inserting this expression into (81) yields

$$\mathrm{i}\dot{\boldsymbol{\Psi}}_0(t) + \mathrm{i}\frac{\mathrm{d}}{\mathrm{d}t}\delta\boldsymbol{\Psi}(t) = \boldsymbol{f}(\boldsymbol{\Psi}_0(t) + \delta\boldsymbol{\Psi}(t)). \tag{85}$$

Using (82), one finds

$$\mathrm{i}\frac{\mathrm{d}}{\mathrm{d}t}\delta\boldsymbol{\Psi} = M\delta\boldsymbol{\Psi} - \mathrm{i}\dot{\boldsymbol{\Psi}}_0, \tag{86}$$

where M is a matrix with the elements $M_{ij} = \frac{\partial f_i}{\partial \psi_j}$ with $i, j = \mathrm{a}, \mathrm{e}, \mathrm{g}$. Here, the partial derivatives are calculated in the dark state. In system (86), the nonlinear terms have been omitted.

Specifically, for the system ((77)–(79)), the matrix M reads

$$M = \begin{pmatrix} 0 & \Omega_\mathrm{p}\psi_\mathrm{a}^{0*} & 0 \\ \Omega_\mathrm{p}\psi_\mathrm{a}^0 & -(\Delta + \mathrm{i}\gamma) & \Omega_\mathrm{d}/2 \\ 0 & \Omega_\mathrm{d}/2 & 0 \end{pmatrix}. \tag{87}$$

(See also (7) in [23].) It is similar to the Hamiltonian (9) of the linear lambda system. The difference is that the elements M_ae and M_ea contain the component of the dark state ψ_a^0 due to the nonlinearity.

Denoting the Jacobian as $A = -\mathrm{i}M$, we can rewrite the linearized equation (86) as

$$\frac{\mathrm{d}}{\mathrm{d}t}\delta\boldsymbol{\Psi} = A\delta\boldsymbol{\Psi} - \dot{\boldsymbol{\Psi}}_0. \tag{88}$$

In this system, the real parts of the eigenvalues of the Jacobian A determine the stability of the dark state. If the matrix M has eigenvalues ω, the Jacobian A has the eigenvalues $\lambda = -\mathrm{i}\omega$. In analogy to the linear lambda system, the eigenvalues ω can be found from the characteristic equation

$$\det||M - I\omega|| = 0. \tag{89}$$

Solving (89) with (87), we find that one root is always zero:

$$\omega_1 = 0. \tag{90}$$

The other two eigenvalues obey the quadratic equation:

$$\omega^2 + (\Delta + \mathrm{i}\gamma)\omega - \left(\Omega_\mathrm{d}^2 + 4\Omega_\mathrm{p}^2\left|\psi_\mathrm{a}^0\right|^2\right)/4 = 0. \tag{91}$$

The corresponding eigenvalues ω_2 and ω_3 obey the following:

$$\omega_2 + \omega_3 = -(\Delta + \mathrm{i}\gamma), \tag{92}$$

$$\omega_2\omega_3 = -\left(\Omega_\mathrm{d}^2 + 4\Omega_\mathrm{p}^2\left|\psi_\mathrm{a}^0\right|^2\right)/4. \tag{93}$$

By setting $\Delta = 0$, we obtain the solutions of quadratic equation:

$$\omega_{2,3} = \left[-\mathrm{i}\gamma \pm \left(-\gamma^2 + \Omega_\mathrm{d}^2 + 4\Omega_\mathrm{p}^2\left|\psi_\mathrm{a}^0\right|^2\right)^{1/2}\right]/2. \tag{94}$$

(see also the equations under (7) in [23]).

In figure 7, we show the dynamics of $\mathrm{Re}(\lambda(t))$ for the nonlinear lambda system. One can see that this picture reproduces the same behaviour as the corresponding dependence for the linear lambda system shown in figure 2. This means that the real parts of eigenvalues of the Jacobian for the nonlinear lambda system are the same as those for the linear system in the corresponding time intervals: $t < t_1, t > t_2$ and $t_1 < t < t_2$.

We now adiabatically eliminate the excited state by setting $\dot{\psi}_\mathrm{e} = 0$. From (78), we obtain

$$\psi_\mathrm{e} = \frac{1}{2(\Delta + \mathrm{i}\gamma)}(\Omega_\mathrm{p}\psi_\mathrm{a}^2 + \Omega_\mathrm{d}\psi_\mathrm{g}). \tag{95}$$

Inserting this result into (77) and (79), we obtain a second-order system:

$$\mathrm{i}\dot{\psi}_\mathrm{a} = \Omega_\mathrm{p}\psi_\mathrm{a}^*\psi_\mathrm{e}, \tag{96}$$

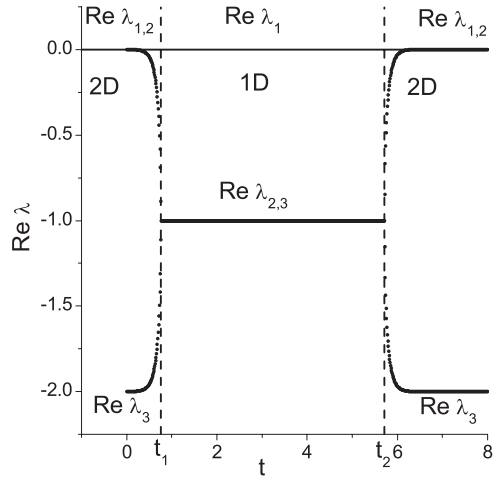

Figure 7. Dynamics of real parts of eigenvalues of the Jacobian for the nonlinear lambda system, computed by (94) and (90). The dashed vertical lines set the boundaries for the 1D and 2D processes. Here, $t_1 = 0.76$ and $t_2 = 5.71$. The parameters are as follows: $\Delta = 0$, $\gamma = 2.0$, $\Omega_0 = 300.0$, $t_p = 3.8$ and $t_d = 3.0$.

$$\mathrm{i}\dot{\psi}_g = \tfrac{1}{2}\Omega_d\psi_e. \tag{97}$$

with ψ_e given by (95).

We now discuss the validity of 3D and 2D systems. The 3D system ((77)–(79)) is valid for all times. In the ranges $t < t_1$ and $t > t_2$, the 2D system ((96), (97)) can be applied since there are two zero real parts $\mathrm{Re}(\lambda_{1,2}) = 0$, and one negative real part $\mathrm{Re}(\lambda_3) \simeq -\gamma$. In the range $t_1 < t < t_2$, the process is 1D since there is only one zero real part $\mathrm{Re}(\lambda_1) = 0$ and two negative real parts $\mathrm{Re}(\lambda_{2,3}) = -\gamma/2$. However, here we do not have any 1D equation, one can only propose the 2D system ((96), (97)). The search for a 1D system is a challenging problem.

In figure 8, we have plotted the relevant dynamics for the case of the adiabatically reduced nonlinear lambda system. In figure 8(a), we show the Gaussian pulses that are ordered counter-intuitively. From figure 8(b), one may conclude that the solutions of the adiabatically reduced system are in good quantitative agreement with the solutions of the exact system (we do not distinguish them in the figure). In figure 8(c), we see that the difference for P_e between exact and approximated solutions is significant. It can be explained by the fact that the magnitude of probability P_e is small. On the other hand, the difference in the case of P_a and P_g is of the same order but we do not distinguish it, since the magnitudes of these quantities are much larger. In figure 8(d), we have plotted the dynamics of the difference between the exact (P_a) and adiabatically reduced (P_a^{ad}) solutions of the population P_a. (See also the blue line in figure 2(c) in [25].) The difference is of the same order as that in figure 8(c).

In figure 9, we have plotted the dynamics of differences between the populations of the current state and corresponding dark state. The difference for the initial ground state a deviates up to 0.03 at the end of the passage. Whereas the difference for the excited state remains much less. The corresponding difference for state g is almost symmetric to that of the state a with respect to zero (not shown here). We conclude that the process is adiabatic since the solution remains in a close neighbourhood to the dark state.

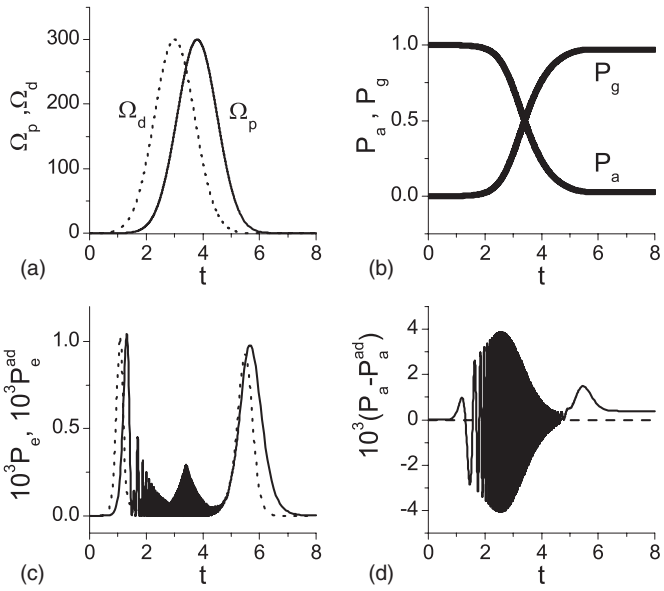

Figure 8. The dynamics (a) of Gaussian pulses (6) and (7), (b) of populations P_a and P_g, (c) of population P_e in enlarged scale and (d) the difference of P_a between exactly (P_a) and adiabatically (P_a^{ad}) obtained solutions. In (b) and (c) the solid thin lines represent the solutions of exact (77)–(79), and the (solid thick/dotted) lines are the solutions of the adiabatically reduced system ((96), (97)) with the excited state given by (95). The parameters are the same as in figure 7. The initial conditions are $\psi_a(0) = 1$, $\psi_g(0) = \psi_e(0) = 0$.

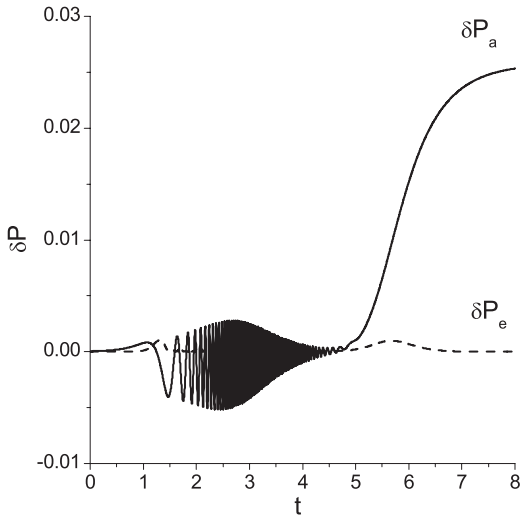

Figure 9. The dynamics of the differences of populations between the current state and the dark state, for $\delta P_a(t) = |\psi_a(t)|^2 - |\psi_a^0(t)|^2$ (solid line), and $\delta P_e(t) = 2|\psi_e(t)|^2$ (dashed line) for the nonlinear lambda system. The dynamics of $\psi_a(t)$, $\psi_e(t)$ are computed from (77) to (79) and $\psi_a^0(t)$ is given by (83). The parameters are the same as in figure 7. The initial conditions are $\psi_a(0) = 1$, $\psi_g(0) = \psi_e(0) = 0$.

5. The nonlinear tripod

We consider the atom–molecule transition in ultracold quantum gases via PA. This problem has potential applications during the creation of ultracold molecules and quantum superchemistry. The underlying physics is closely related to

the STIRAP and has been widely studied in the context of atomic physics and quantum optics [3, 52].

The level structure of the atom–molecule tripod system is shown in figure 3. In ultracold atomic systems, the level a denotes the atomic BEC, which couples an excited state of a diatomic molecular BEC via the pump field $\Omega_p(t)$. Such an excited state is represented by high-lying vibration levels of the single excited molecule. The excited state is coupled to the two ground states of the molecular BEC, $g1$ and $g2$, with the strengths $\Omega_{d1}(t)$ and $\Omega_{d2}(t)$, respectively.

Assuming a two-photon resonance condition, the four-level nonlinear Hamiltonian for nonlinear tripod takes the form

$$\hat{H} = -\hbar(\Delta + i\gamma)\hat{\psi}_e^\dagger\hat{\psi}_e + \frac{\hbar}{2}\big(\Omega_p\hat{\psi}_e^\dagger\hat{\psi}_a\hat{\psi}_a + \Omega_{d1}\hat{\psi}_e^\dagger\hat{\psi}_{g1} + \Omega_{d2}\hat{\psi}_e^\dagger\hat{\psi}_{g2} + \text{h.c.}\big). \quad (98)$$

Here, $\hat{\psi}_\alpha$, $\hat{\psi}_\alpha^\dagger$ ($\alpha = a, e, g1, g2$) are the bosonic annihilation and creation operators for the state α, respectively. To explore the behaviour of the system under time evolution, we consider the problem under mean-field approximation, which is reasonable for bosonic systems when the number of particles is large compared with unity [29, 37]. In this limit, the bosonic operators are replaced by c numbers, and the Heisenberg equation leads to the following equations of motion for the probability amplitudes:

$$i\dot{\psi}_a = \Omega_p\psi_a^*\psi_e, \quad (99)$$

$$i\dot{\psi}_e = -(\Delta + i\gamma)\psi_e + \tfrac{1}{2}\Omega_p\psi_a^2 + \tfrac{1}{2}\Omega_{d1}\psi_{g1} + \tfrac{1}{2}\Omega_{d2}\psi_{g2}, \quad (100)$$

$$i\dot{\psi}_{g1} = \tfrac{1}{2}\Omega_{d1}\psi_e, \quad (101)$$

$$i\dot{\psi}_{g2} = \tfrac{1}{2}\Omega_{d2}\psi_e. \quad (102)$$

The nonlinear term enters here when the molecules are obtained via associating cold atoms.

The normalization reads

$$|\psi_a(t)|^2 + 2[|\psi_{g1}(t)|^2 + |\psi_{g2}(t)|^2 + |\psi_e(t)|^2] \leqslant 1, \quad (103)$$

where the equality holds for the initial time.

Like in the case of linear tripod, the Gaussian pulses are given by (40)–(42).

Similar to the linear case, we define the following state vector of the system: $\boldsymbol{\Psi} = [\psi_a, \psi_e, \psi_{g1}, \psi_{g2}]^T$. The dynamic equations (99)–(102) can be rewritten in a vector form given by (81), where $\boldsymbol{f}$ is now the vector of nonlinear functions on the rhs of (99)–(102). The manifold of the steady states of this system represents the dark state $\boldsymbol{\Psi}_0 = [\psi_a^0, \psi_e^0, \psi_{g1}^0, \psi_{g2}^0]^T$. This manifold has to satisfy (82) and the condition of normalization. Since $\psi_e^0 = 0$, the dark state obeys the following:

$$\Omega_p\big(\psi_a^0\big)^2 + \Omega_{d1}\psi_{g1}^0 + \Omega_{d2}\psi_{g2}^0 = 0, \quad (104)$$

$$\big|\psi_a^0\big|^2 + 2\big|\psi_{g1}^0\big|^2 + 2\big|\psi_{g2}^0\big|^2 = 1, \quad (105)$$

$$\psi_e^0 = 0. \quad (106)$$

We are interested in the linear stability of this dark state. Therefore, we suppose that the solutions of (99)–(102) evolve in the close neighbourhood of the dark state $\boldsymbol{\Psi}_0$, i.e. we express it as a sum given by (84) where $\delta\boldsymbol{\Psi}(t)$ is the deviation of the current solution from the dark state. Hence, one arrives at a linearized equation similar to the one for the nonlinear lambda system (86) where the matrix M reads

$$M = \begin{pmatrix} 0 & \Omega_p\psi_a^{0*} & 0 & 0 \\ \Omega_p\psi_a^0 & -[\Delta + i\gamma] & \Omega_{d1}/2 & \Omega_{d2}/2 \\ 0 & \Omega_{d1}/2 & 0 & 0 \\ 0 & \Omega_{d2}/2 & 0 & 0 \end{pmatrix}. \quad (107)$$

Note that this matrix is very similar to the Hamiltonian (43) for the linear tripod. The main difference between them is dependence of M on ψ_a^0 that arises due to the nonlinearity. On the other hand, this matrix is also similar to the corresponding matrix for the nonlinear lambda system. The Jacobian of the linearized system is given by $A = -iM$. The eigenvalues ω of the matrix M correspond to eigenvalues $\lambda = -i\omega$ of Jacobian. Solving the eigenvalues problem for matrix M, we obtain two zero eigenvalues:

$$\omega_{1,2} = 0. \quad (108)$$

The other two eigenvalues can be found from the quadratic equation

$$\omega^2 + (\Delta + i\gamma)\omega - \big(\Omega_{d1}^2 + \Omega_{d2}^2 + 4\Omega_p^2\big|\psi_a^0\big|^2\big)/4 = 0. \quad (109)$$

The eigenvalues $\omega_{3,4}$ satisfy the condition

$$\omega_3 + \omega_4 = -(\Delta + i\gamma), \quad (110)$$

$$\omega_3\omega_4 = -\big(\Omega_{d1}^2 + \Omega_{d2}^2 + 4\Omega_p^2\big|\psi_a^0\big|^2\big)/4. \quad (111)$$

We again assume that $\Delta = 0$, thus obtaining the following solutions:

$$\omega_{3,4} = \big[-i\gamma \pm \big(-\gamma^2 + \Omega_{d1}^2 + \Omega_{d2}^2 + 4\Omega_p^2\big|\psi_a^0\big|^2\big)^{1/2}\big]/2. \quad (112)$$

In figure 10(b), we plot the dynamics of eigenvalues of the Jacobian for the nonlinear tripod. The way of finding the eigenvalues is discussed below. As we saw above, the behaviours of corresponding eigenvalues for the linear and nonlinear lambda systems was the same. Comparing figures 10(b) and 4, we see that here one can make an identical conclusion: the roots behave in the same manner for the linear and nonlinear tripods.

Now we discuss computing the dynamics of the real parts of eigenvalues, i.e. $\mathrm{Re}(\lambda) = \mathrm{Re}(\lambda(t))$. The matrix M in the present case depends on ψ_a^0, (see M_{ae} and M_{ea} in (107)). In the case of the nonlinear lambda system, the dark state was uniquely defined as a function of Rabi frequencies (83). However, in this case, for the nonlinear tripod, the dark state is a manifold that is given by (104)–(106). But we need a definite function of time $\psi_a^0 = \psi_a^0(t)$ in order to get the dynamics of eigenvalues. Therefore, we use the parametrization of the dark state that was derived in [32]. If the solutions of (99)–(102) evolves on the dark-state manifold, we may express the solution in terms of only two variables (parameters), $[u_1(t), u_2(t)]$:

$$\psi_a^0 = \left[\frac{\delta_p}{\cos(\Theta)}\right]^{1/2} u_2^{1/2}, \quad (113)$$

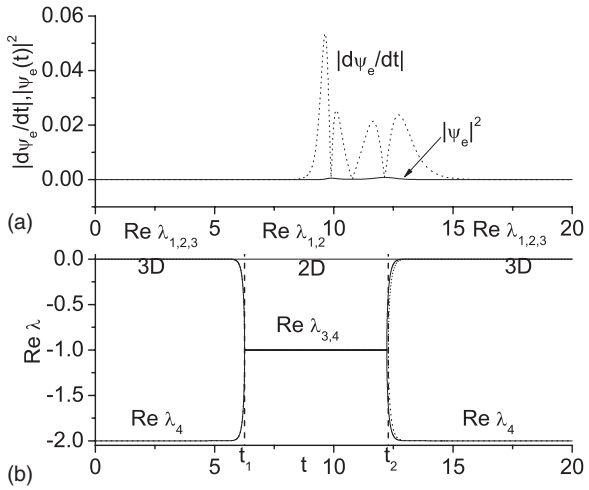

Figure 10. (a) Dynamics of $|\dot{\psi}_e(t)|$ (dotted) and $|\psi_e(t)|^2$ (solid) for nonlinear tripod, both computed by (99)–(102); (b) dynamics of real parts of eigenvalues of the Jacobian for nonlinear tripod, computed by (112) and (108). The solid lines are the exact roots, and the dotted lines correspond to stability of the current solution (see the text for details). The dashed black vertical lines set the boundaries for the 3D and 2D processes. Here, $t_1 = 6.26$ and $t_2 = 12.29$. The parameters are as follows: $\Delta = 0$, $\gamma = 2.0$, $\Omega_0 = 60.0$, $t_p = 10.7$, $t_{d1} = 10.0$, $t_{d2} = 8.5$, $K_1 = 0.75$ and $K_2 = 5.0$. The initial conditions are $\psi_a(0) = 1$, $\psi_{g1}(0) = \psi_{g2}(0) = \psi_e(0) = 0$.

$$\psi^0_{g1} = u_1 \sin(\Theta) - u_2 \cos(\Theta), \tag{114}$$

$$\psi^0_{g2} = -u_1 \cos(\Theta) - u_2 \sin(\Theta). \tag{115}$$

(See the system of equations before (17) in [32].) Here, $\delta_p = \Omega_{d1}/\Omega_p$ and Θ are defined by $\tan(\Theta) = \Omega_{d2}/\Omega_{d1}$. In [32], it was also shown that in the adiabatic limit, the parameters should obey the equations (see (17) in [32])

$$\dot{u}_1 + \dot{\Theta} u_2 = 0, \tag{116}$$

$$\dot{u}_2 \left(1 + \frac{\delta_p}{4u_2 \cos(\Theta)}\right) - \dot{\Theta} u_1 + \frac{d}{dt}\left[\frac{\delta_p}{4\cos(\Theta)}\right] = 0. \tag{117}$$

We integrate the system ((116), (117)) and insert its solution in the parametrization (113), thus obtaining the necessary dynamics of $\psi^0_a(t)$. After inserting this dynamics in (112), we obtain the dynamics of eigenvalues of the Jacobian for the nonlinear tripod system.

We may also suppose that the deviation for the amplitude ψ_a is almost zero, $\delta\psi_a(t) \simeq 0$. We thus can make a substitution into (110), (111) and (112):

$$\psi^0_a \to \psi_a. \tag{118}$$

Subsequently, one can numerically solve the system ((99)–(102)). By inserting $\psi_a(t)$ into (110), (111) and (112), one obtains the approximate dynamics of the eigenvalues. Actually, this approach means the analysis of the stability of the current solution $\mathbf{\Psi}(t) = [\psi_a(t), \psi_e(t), \psi_{g1}(t), \psi_{g2}(t)]^T$. The dynamics of $|\dot{\psi}_e(t)|$ and $|\psi_e(t)|^2$ is plotted in figure 10(a). The first dynamics indicates that the magnitude of the rhs of (100) is of the order of 0.06. The second dynamics shows that the excited level remains almost unpopulated throughout the passage. We therefore conclude that the process is almost adiabatic, and one may justify the substitution (118).

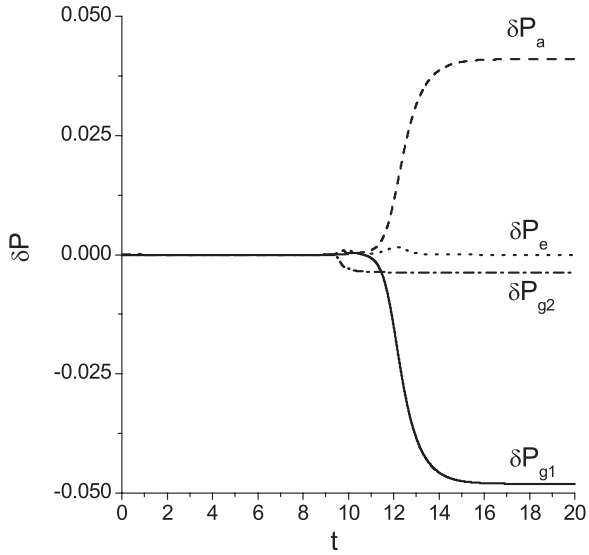

Figure 11. The dynamics of the differences of populations between the current state and the dark state for the nonlinear tripod, $\delta P_a(t) = |\psi_a(t)|^2 - |\psi^0_a(t)|^2$ (dashed line), $\delta P_e(t) = 2|\psi_e(t)|^2$ (dotted line), $\delta P_{g1}(t) = 2|\psi_{g1}(t)|^2 - 2|\psi^0_{g1}(t)|^2$ (solid line), and $\delta P_{g2}(t) = 2|\psi_{g2}(t)|^2 - 2|\psi^0_{g2}(t)|^2$ (dash-dotted line). The dynamics of $\psi_a(t)$, $\psi_e(t)$, $\psi_{g1}(t)$ and $\psi_{g2}(t)$ are computed from (99) to (102), and $\psi^0_a(t)$, $\psi^0_{g1}(t)$, $\psi^0_{g2}(t)$ are found from (113) to (115) and (116) and (117). The parameters are the same as in figure 10. The initial conditions are $\psi_a(0) = 1$, $\psi_{g1}(0) = \psi_{g2}(0) = \psi_e(0) = 0$.

In figure 10(b), we plot the dynamics of $\mathrm{Re}(\lambda(t))$ computed by both the ways. The solid line shows the dynamics of $\mathrm{Re}(\lambda(t))$ computed by using the exact value of $\psi^0_a(t)$, and the dotted line displays the approximate dynamics that is obtained by using the substitution (118). We can see from figure 10(b) that the stability of the current solution (dotted line) is identical to that of the dark state at the beginning and middle of the process. However, the splitting of the real parts for the approximate eigenvalues is slightly delayed with respect to the exact ones. The good quantitative agreement of both results confirms the validity of approximation (118); it also shows that the current solution evolves in the close neighbourhood of the moving dark state (113)–(115).

Exactly as in the previous sections, we adiabatically eliminate the excited state by setting $\dot{\psi}_e = 0$. From (100), we obtain

$$\psi_e = \frac{1}{2(\Delta + i\gamma)}\left(\Omega_p \psi_a^2 + \Omega_{d1}\psi_{g1} + \Omega_{d2}\psi_{g2}\right). \tag{119}$$

Inserting this expression into (99), (101) and (102), we obtain

$$i\dot{\psi}_a = \Omega_p \psi^*_a \psi_e, \tag{120}$$

$$i\dot{\psi}_{g1} = \tfrac{1}{2}\Omega_{d1}\psi_e, \tag{121}$$

$$i\dot{\psi}_{g2} = \tfrac{1}{2}\Omega_{d2}\psi_e. \tag{122}$$

In these equations, we use the expression of ψ_e given by (119).

In figure 11, we have depicted the dynamics of the deviations of the current populations from those of the dark state. One can see that all three populations deviate up to 0.05 showing that the solution remains in a proximity to the dark-state manifold. Therefore, one may conclude that the process is adiabatic.

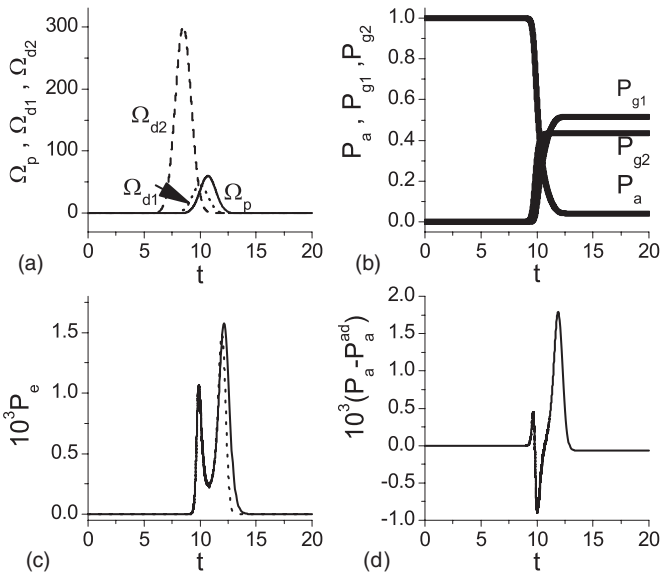

Figure 12. The dynamics (a) of Gaussian pulses (40)–(42), (b) of populations P_a, P_{g1}, P_{g2} and (c) of population P_e in an enlarged scale. In (d), it is shown as the difference between the exact (P_a from (99) to (102)) and adiabatically reduced (P_a^{ad} from (120) to (122)) populations in the enlarged scale. In (b) and (c), the solid thin lines represent the solutions of exact (99)–(102), and the (solid thick/dotted) lines are the solutions of the adiabatically reduced system ((120)–(122)) with the excited state given by (119). The parameters are as follows: $\Delta = 0$, $\gamma = 2.0$, $\Omega_0 = 60.0$, $t_p = 11.5$, $t_{d1} = 10.0$, $t_{d2} = 8.5$, $K_1 = 0.75$ and $K_2 = 5.0$. The initial conditions are the same as in figure 10.

In figure 12, we have plotted the dynamics for the case of the nonlinear tripod. Figure 12(a) shows a sequence of Gaussian pulses. In figure 12(b), we show the dynamics of populations of the levels. The solutions of the approximated system are in good quantitative agreement with those of the exact system (in the figure we do not distinguish them). From figure 12(c), we see that the population of the excited state is reproduced by the approximated system with a significant error. Again, as in the previous section, we explain this fact by small magnitude of quantity P_e. In figure 12(d), we have plotted the difference between exact (P_a) and adiabatically approximated (P_a^{ad}) population P_a. It is of the same order as in the case of the excited state (see figure 12(c)).

6. Some remarks about the one-photon detuning

To date, we have been setting $\Delta = 0$ for all considered systems. In this section, we shall explore a behaviour of the system in the presence of the non-zero one-photon detuning $\Delta \neq 0$. In that case, when solving the quadratic equations for the eigenvalues of the Jacobians, one obtains the complex-valued discriminants, $D \equiv |D|\,e^{i\varphi}$, where $|D|$ is their real amplitude and φ is their phase. The eigenvalues of the Jacobian then read

$$\lambda_{3,4} = \left[-\frac{1}{2}\gamma \pm \frac{1}{2}|D|^{1/2}\sin\left(\frac{\varphi}{2}\right)\right] + i\left[\frac{1}{2}\Delta \mp \frac{1}{2}|D|^{1/2}\cos\left(\frac{\varphi}{2}\right)\right]. \quad (123)$$

Here, the real and imaginary parts of the discriminant are given by

$$\mathrm{Re}(D) = \Delta^2 - \gamma^2 + \Omega_{d1}^2 + \Omega_{d2}^2 + 4\Omega_p^2|\psi_a^0|^2, \quad (124)$$

$$\mathrm{Im}(D) = 2\gamma\Delta. \quad (125)$$

These equations are valid for the nonlinear tripod; for the other systems, we obtain similar expressions. If $\Delta = 0$ (as assumed previously), the imaginary part becomes zero, i.e. $\mathrm{Im}(D) = 0$; the phase may be either 0 or π; in the interval $t_1 < t < t_2$, it is $\varphi = 0$, and in the ranges $t < t_1$, $t > t_2$ it is $\varphi = \pi$. For $\varphi = 0$, we have $\mathrm{Re}(\lambda_{3,4}) = -\gamma/2$, and for $\varphi = \pi$, we obtain $\mathrm{Re}(\lambda_3) \simeq 0$, $\mathrm{Re}(\lambda_4) \simeq -\gamma$. We have obtained these results for all the considered systems (see e.g. figure 10(b)). However, in the case of the non-zero one-photon detunings, in the interval $t_1 < t < t_2$, these real parts are no longer coinciding; they are symmetrically surrounding the value $-\gamma/2$, and the difference between them becomes equal to

$$\mathrm{Re}\,\lambda_3 - \mathrm{Re}\,\lambda_4 = |D|^{1/2}\sin\left(\frac{\varphi}{2}\right) \simeq \frac{\mathrm{Im}(D)}{2[\mathrm{Re}(D)]^{1/2}}. \quad (126)$$

The latter approximation is valid for the small values of $\mathrm{Im}(D) \ll \mathrm{Re}(D)$. Such a situation takes place in the middle of the passage, when the Rabi frequencies are large compared to the one-photon detuning and losses.

We thus conclude that for such small detunings, the difference between the negative real parts remains small, and our statements about the reduction of dimension remain valid.

7. Conclusions

We have analysed the adiabatic reduction of the dimension of the linear and nonlinear three- and four-level systems. By evaluating the corresponding Jacobians and computing the dynamics of real parts of their eigenvalues (the non-zero eigenvalues are found from quadratic characteristic equations), one may define the dimensionality of the processes. This dimensionality is given by the number of zero real parts since the negative real parts cause the contraction of the nearby solutions towards the dark state. At the beginning and the end of the dynamics, there is always only one negative real part. Hence, one may eliminate only one state representing the excited state. In the middle of the process, one of the zero real parts becomes negative thus making the number of negative real parts equal to two. In this time interval, we may eliminate two variables corresponding to the excited and bright states, respectively. For linear systems, we have eliminated both excited and bright states. However, for nonlinear systems, we have restricted ourselves by eliminating the excited state. This is due to the fact that the definition of a bright state for the nonlinear systems is not available. We suppose that the remaining stable degrees of freedom in the nonlinear systems can be eliminated by using the asymptotic methods of nonlinear dynamics.

The main finding of this work reveals that the whole STIRAP evolution for all considered systems is divided into

three time intervals with a different number of the negative real parts of the Jacobians. The evolution of the real parts is equivalent to the corresponding linear and nonlinear systems (as one can see in figures 2, 4, 7 and 10(b)). This suggests that the nonlinear systems may be potentially reduced as the linear ones. Physically, this means that the considered three/four-level schemes may be regarded as schemes with lower dimension, i.e. with fewer levels involved. In the time intervals $t < t_1$ and $t > t_2$, the initially three-level system is effectively a two-level one, and in the range of $t_1 < t < t_2$ it contains a single level. Analogously, the initially four-level scheme may be regarded as a three-level (two-level) system in the time ranges, where $t < t_1, t > t_2$ ($t_1 < t < t_2$).

A sensitive problem is the definition of a dark state for the nonlinear tripod. In the case of the nonlinear lambda system, the dark state is a moving point (83) in the phase space. However, for the nonlinear tripod, we have a manifold (104)–(106) of dark states. If one wishes to obtain the dynamics of real parts of eigenvalues of the Jacobian, then one needs a definite value of complex amplitude ψ_a^0 belonging to the manifold. We here use two ways for the stability analysis of the dark state. The first way is to parametrize the dark-state manifold by using the method developed in [32]. This method enables one to find the definite dynamics of $\psi_a^0(t)$. We thus managed to find the exact dynamics of eigenvalues. The second way is to simply substitute using (118) the value $\psi_a^0(t)$ by the current solution $\psi_a(t)$ that is found from underlying equations (99)–(102). Actually, the substitution (118) means we are investigating the stability of the current solution instead of that for the dark state. In fact, figure 10(b) shows that the real parts of the eigenvalues evolve almost identically. The only difference is that the splitting of real parts for approximate eigenvalues is slightly delayed. Such a coincidence shows that the current solution evolves in the close neighbourhood to the motion of the parametrized dark state (113)–(115). It is also to be noted that the magnitude of $|\dot{\psi}_e|$ is always small, and the excited state remains almost unpopulated as we can see in figure 10(a).

It is noteworthy that a related approach was used in [30], where a feedback control scheme was presented that designs time-dependent laser-detuning frequency to suppress possible dynamical instability in coupled free-quasibound-bound atom–molecule condensate systems. It was proposed to perform a substitution analogous to (118) which was used for solving the control problem. On the other hand, in our work this substitution was made for the stability analysis of the dark state.

It is also important to note that in the lambda and tripod systems, we have phenomenologically included the loss coefficient γ. This was done by making the one-photon detuning to be a complex number, i.e. by replacing $\Delta \to \Delta + i\gamma$. Here, Δ is again a one-photon detuning and γ determines the losses. In our work, we have considered the cases where $\Delta = 0$ and $\gamma > 0$, i.e. the one-photon resonances with losses. We stress that the presence of non-zero losses γ makes the adiabatic reduction easier to implement. The losses cause the appearance of two negative real parts of eigenvalues of the corresponding Jacobians. On the other hand, it was shown that the losses decrease the transfer efficiency [8], which decreases exponentially with the (small) decay rate. However, the range of decay rates, over which the transfer efficiency remains high, appears to be proportional to the squared pulse area. Hence, by choosing high pulse areas one may preserve the high transfer efficiency.

Another question is a possible presence of the one-photon detuning in the considered processes. As was shown in section 6, the relatively small one-photon detuning does not alter our conclusions about the reduction of dimension in the three- and four-level systems considered here. This happens if the Rabi frequencies are large compared to the one-photon detuning and loss rates.

Acknowledgments

The authors acknowledge the support by the EU FP7 project STREP NAMEQUAM.

References

[1] Bergmann K, Theuer H and Shore B W 1998 *Rev. Mod. Phys.* **70** 1003–25
[2] Vitanov N V, Halfmann T, Shore B W and Bergmann K 2001 *Annu. Rev. Phys. Chem.* **52** 763–809
[3] Vitanov N V, Fleischhauer M, Shore B W and Bergmann K 2001 *Adv. At. Mol. Opt. Phys.* **46** 55–190
[4] Arimondo E 1996 *Progress in Optics* vol 35 ed E Wolf (Amsterdam: Elsevier) p 259
[5] Kral P, Thanapulos I and Shapiro M 2007 *Rev. Mod. Phys.* **79** 53–77
[6] Oreg J, Hioe F T and Eberley J H 1984 *Phys. Rev.* A **29** 690–7
[7] Carrol C E and Hioe F T 1988 *J. Opt. Soc. Am.* B **5** 1335–40
[8] Vitanov N V and Stenholm S 1997 *Phys. Rev.* A **56** 1463–71
[9] Unanyan R G, Yatsenko L P, Bergmann K and Shore B W 1997 *Opt. Commun.* **139** 43–7
[10] Ivanov P A, Vitanov N V and Bergmann K 2004 *Phys. Rev.* A **70** 063409
[11] Ivanov P A, Vitanov N V and Bergmann K 2005 *Phys. Rev.* A **72** 053412
[12] Vasilev G S, Kuhn A and Vitanov N V 2009 *Phys. Rev.* A **80** 013417
[13] Unanyan R, Fleischhauer M, Shore B W and Bergmann K 1998 *Opt. Commun.* **155** 144–54
[14] Unanyan R G, Shore B W and Bergmann K 1999 *Phys. Rev.* A **59** 2910–9
[15] Lazarou C and Vitanov N V 2010 *Phys. Rev.* A **82** 033437
[16] Theuer H, Unanyan R G, Habscheid C, Klein K and Bergmann K 1999 *Opt. Express* **4** 77–83
[17] Goto H and Ichimura K 2007 *Phys. Rev.* A **75** 033404
[18] Kis Z, Vitanov N V, Karpati A, Barthel C and Bergman K 2005 *Phys. Rev.* A **72** 033403
[19] Garcia-Fernandez R, Shore B W, Bergmann K, Ekers A and Yatsenko L P 2006 *J. Chem. Phys.* **125** 014301
[20] Winkler K, Thalhammer G, Theis M, Ritsch H, Grimm R and Denschlag J H 2005 *Phys. Rev. Lett.* **95** 063202
[21] Moal S, Portier M, Kim J, Dugue J, Rapol U D, Leduc M and Tanoudji C C 2006 *Phys. Rev. Lett.* **96** 023203
[22] Ling H Y, Pu H and Seaman B 2004 *Phys. Rev. Lett.* **93** 250403
[23] Pu H, Maenner P, Zhang W and Ling H Y 2007 *Phys. Rev. Lett.* **98** 050406
[24] Ling H Y, Maenner P, Zhang W and Pu H 2007 *Phys. Rev.* A **75** 033615
[25] Itin A P and Watanabe S 2007 *Phys. Rev. Lett.* **99** 223903

[26] Itin A P, Watanabe S and Konotop V V 2008 *Phys. Rev.* A **77** 043610
[27] Hope J J, Olsen M K and Plimak L I 2001 *Phys. Rev.* A **63** 043603
[28] Meng S Y, Fu L B and Liu J 2008 *Phys. Rev.* A **78** 053410
[29] Mackie M, Kowalski R and Javanainen J 2000 *Phys. Rev. Lett.* **84** 3803–6
[30] Cheng J, Han S and Yan Y 2006 *Phys. Rev.* A **73** 035601
[31] Zhao C, Zou X B, Pu H and Guo G C 2008 *Phys. Rev. Lett.* **101** 010401
[32] Zhou X F, Zhang Y S, Zhou Z W and Guo G C 2010 *Phys. Rev.* A **81** 043614
[33] Sarandy M S and Lidar D A 2005 *Phys. Rev.* A **71** 012331
[34] Amin M H S 2009 *Phys. Rev. Lett.* **102** 220401
[35] Haken H 1983 *Synergetics* (Berlin: Springer)
[36] Wu J H, Cui C L, Ba N, Ma Q R and Gao J Y 2007 *Phys. Rev.* A **75** 043819
[37] Mackie M, Collin A and Javanainen J 2005 *Phys. Rev.* A **71** 017601
[38] Liu J, Wu B and Niu Q 2003 *Phys. Rev. Lett.* **90** 170404
[39] Jing H, Cheng J and Meystre P 2007 *Phys. Rev. Lett.* **99** 133002
[40] Jing H and Jiang Y 2008 *Phys. Rev.* A **77** 065601
[41] Jing H, Cheng J and Meystre P 2008 *Phys. Rev.* A **77** 043614
[42] Jing H, Zheng F, Jiang Y and Geng Z 2008 *Phys. Rev.* A **78** 033617
[43] Eckert K, Lewenstein M, Corbalan R, Birkl G, Ertmer W and Mompart J 2004 *Phys. Rev.* A **70** 023606
[44] Pazy E, Tikhonenkov I, Band Y B, Fleischhauer M and Vardi A 2005 *Phys. Rev. Lett.* **95** 170403
[45] Larson J 2011 *Eur. Phys. Lett.* **96** 50004
[46] Jing H, Deng Y and Meystre P 2011 *Phys. Rev.* A **83** 063605
[47] Zhang X F, Chen J C, Li B, Wen L and Liu W M 2011 arXiv:1108.5000
[48] Kis Z and Renzoni F 2002 *Phys. Rev.* A **65** 032318
[49] Meng S Y, Fu L B, Chen J and Liu J 2009 *Phys. Rev.* A **79** 063415
[50] Ivanov S S and Vitanov N V 2011 *Opt. Lett.* **36** 1275–7
[51] Renzoni F, Maichen W, Windholz L and Arimondo E 1997 *Phys. Rev.* A **55** 3710
[52] Hioe F T and Eberly J H 1984 *Phys. Rev.* A **29** 1164